Insertion Mechanism of N_2 and O_2 into T_n(n = 8, 10, 12)-Silsesquioxane Framework

Baudilio Tejerina and Mark S. Gordon*

Department of Chemistry, Iowa State University, Ames, Iowa 50011

Received: June 25, 2002; In Final Form: September 6, 2002

The process of insertion of molecular oxygen and nitrogen into polyhedral oligomeric silsesquioxanes (POSS) has been investigated theoretically. Using ab initio methods, the N_2 interaction with the POSS has been described with restricted Hartree−Fock (RHF) with a triple-ζ basis set, while systems involving O_2 require restricted open shell (ROHF) wave functions, to account for their open-shell ground states. This insertion process is described in terms of the energetic change that the system X_2::POSS undergoes when the gas molecule passes from the exterior to the interior of the cage through the largest of its faces. The formation of the cluster occurs through a transition structure that has been characterized for each system. The barrier is a function of the dimension of the face of the POSS and, hence, of the cage dimensions. The results of the calculation are consistent with experimental observations that the O_2 molecules pass through a given membrane more easily than N_2.

Introduction

Polyhedral oligomeric silsesquioxanes (POSSs) have been known for many years.[1] In the last few decades, they have become increasingly important for a variety of applications. For this reason, the processes of POSS synthesis have lately undergone a large development passing from a small amount production in laboratories to larger industrial scale quantities.[2]

The identification and characterization of POSS are normally accomplished in solution (IR and NMR) solid state (X-ray and neutron diffraction) and gas phase (mass spectroscopy).[3−6] Theoretical techniques may be applied to complement and to provide insight to the experimental results. For example, the mechanism of synthesis and reaction of POSSs have been studied by theoretical means.[7] The design and prediction of the structure and stability of other types of POSS have also been supported by theory.[8,9]

Because of their nanostructure nature and their ceramic-like properties (creep and oxidation resistant), POSSs are being used in the synthesis of polymer-derived ceramics.[10] Additionally, they constitute the basic reagent for the preparation of hybrid (inorganic−organic) polymers.[11] Recently, they have been used in the construction of microelectronic mechanical systems[12] and fabrication of microoptical devices.[13] They serve as excellent models to mimic the "functions" of zeolites; for example, gallosiloxanes are analogous to the building units of zeolites.[14] Metal-containing silsesquioxanes, oligometalla-silsesquioxanes, function as catalytic converters for homogeneous catalysts for olefin processing: metathesis, epoxidation, and polymerization of alkenes are easily accomplished with POSS derivatives.[15] Similarly, POSSs are also being used as models for heterogeneous silica-supported catalysts.[16] They have also found application as supporters for the Ziegler−Natta catalysts.[17] In optics, they have a fruitful area of applicability as liquid crystals.[18] They have also been proposed as possible NLO species due to their high transparency,[19] as models for oxo-surfaces in micro-[20] and mesoporous silica,[21]and as metal surface and cluster additives for silicon,[22] iron,[23] and gold.[24]

The cage-like molecular structure of POSS makes them potentially useful substances for separating mixtures of gases as has been observed in siloxanes[25] and silicon-based capillary membranes.[26] It is experimentally known that silicone rubber, as poly(dimethylsiloxane), presents a large permeability to oxygen molecules compared with those of nitrogen.[27] The observed permselectivity makes these compounds useful materials for the separation of N_2/O_2 mixtures.[28] These observations have been attributed to the difference in size of the two molecules: the O_2 has a smaller molecular sieving radius compared to N_2. However, the empirical covalent atomic radii of oxygen and nitrogen are very similar (0.73 and 0.75 Å respectively),[29] so the observed selectivity may be due to other factors as well.

The focus of this paper is on the study of how the structure and the topography of POSS faces can affect and possibly be used to control the absorption of small X_2 molecules nitrogen and oxygen.

Computational Details

Geometry optimizations were performed using Hartree−Fock calculations and the TZV(d,p)[30] basis set. Restricted Hartree−Fock (RHF) and restricted open shell Hartree−Fock (ROHF) were employed for closed- and open-shell species, respectively.

The symbol "$\mathbf{T}_n$" will be used to name the POSS that contains n silsesquioxenyl ($HSiO_{3/2}$) units. The symbol "D_m" will denote the faces of the POSS containing m silicon atoms. In addition, the nomenclature of a POSS may be complemented by providing the symmetry point group it belongs to and also the characteristic topological descriptor $\{r^s\cdots t^u\}$, which indicates the number s-of r-membered rings (faces) that comprises the polyhedron $\mathbf{T}_n$.[3] Each system that involves interaction between the X_2 molecule and the POSS (namely, the cluster or transition structures) will be referred to as X_2::$\mathbf{T}_n$.

The optimization of the molecular geometries of all $\mathbf{T}_n$ systems was performed in natural internal coordinates,[31] while Cartesian coordinates have been used for the clusters and transition structures X_2::$\mathbf{T}_n$. For each equilibrium nuclear configuration (gradient of the energy no larger than 10^{-6} hartree/bohr), the structure was characterized by the analysis of the Hessian (matrix of the energy second derivatives with respect

10.1021/jp021490f CCC: $22.00
Published on Web 10/12/2002

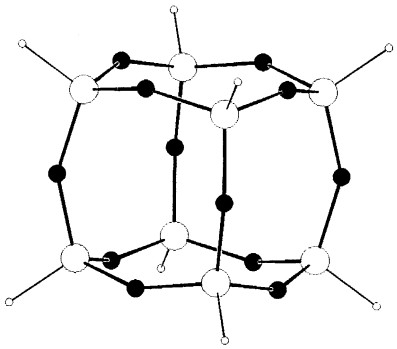

Figure 1. Theoretical structure, O_h, of $\mathbf{T_8}$-POSS.

TABLE 1: Selected Geometry Parameters (Angstroms and degrees), Measured and Calculated for T_8-Poss

	calcd[a]	exptl[b]	calcd[c]
Si−H	1.455	1.461(4)	
Si−O	1.624	1.625(2)	1.64(1.68)
H−Si−O	110.5	109.5(1)	
Si−O−Si	150.5	147.3(1)	146.5(144.6)
O−Si−O	108.4	109.4(1)	110.4(111.3)

[a] This work. RHF/TZV(d,p). [b] Neutron diffraction, from ref 36. Standard deviations in parentheses. [c] From ref 37: Local and nonlocal (in parentheses) density approximation DFT with frozen-core double-ζ basis set.

to the nuclear coordinates). All structures were thereby identified as local minima or transition structures (TS) on their potential energy surfaces (PES).

Electron correlation was taken into account using single point second-order Møller−Plesset perturbation theory (MP2)[32] calculations at each stationary point. This work has been accomplished by the parallel MP2 method [33,34] in GAMESS.[35]

Results and Discussion

A. $\mathbf{T_8}$. The POSS-$\mathbf{T_8}$, $(SiHO_{3/2})_8$, has been broadly studied experimentally and theoretically. In solution, ^{1}H- and ^{29}Si NMR experiments show unique signals in both spectra, which reveal an octahedral structure.[3] In the solid, however, its structure, determined by neutron diffraction at 29 ± 0.5 K, belongs to the T_h point group.[36] To investigate these differences, we have assessed the symmetry of $\mathbf{T_8}$ in the gas phase, studying four possible structures: C_{4v}, D_{4h}, T_d, and O_h. All of them converged to the same O_h geometry with a topological descriptor $\{4^6\}$ (Figure 1).

The molecular structure in the crystal, despite being T_h, is very close to O_h symmetry. A comparison of the predicted and experimental geometries is presented in Table 1 where it may be seen that the agreement between theory and experiment is very good. The HF split-valence plus polarization study reported by de Man and Sauer predict a Si−O distance of 1.64 Å.[8c] Tossell has calculated the HF/6-31G* structure of $\mathbf{T_8}$ and found a Si−O distance of 1.619 Å.[9] Using DFT-based methods with a double-ζ basis set, Xiang et al. have studied the molecular and electronic structure of $\mathbf{T_n}$-POSS (n even, 4−16).[37] Although the calculated symmetry of the $\mathbf{T_8}$-POSS is O_h, the dimension of each D_4 face and the volume of the POSS are slightly larger than those predicted in the present study, as shown in Table 1. Pasquarello et al.,[22c] using LDA-DFT with effective core potentials (ECP) have obtained results (Si−O 1.62 Å) very close to the experimental X-ray diffraction values (Si−O 1.62 Å).[38] However, DFT-B3LYP calculations with the SBKJC-ECP basis set performed in this laboratory predict that the O_h structure of the $\mathbf{T_8}$-POSS corresponds to a second-order saddle point, which relaxes to a less symmetric D_{4h} structure that is 0.5 kcal/mol lower in energy. It is concluded that the HF/double-ζ level of theory is a reasonable approach for the gas-phase geometry optimizations. It is anticipated that an accurate description of their interaction with X_2 will require larger basis sets.

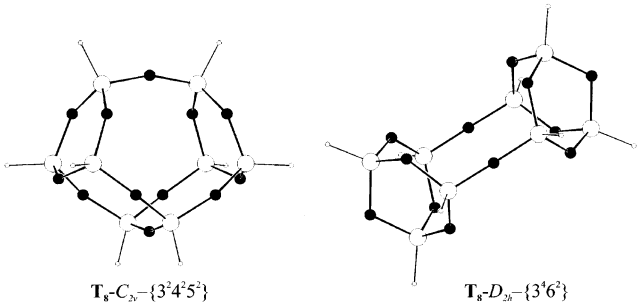

Figure 2. Structural isomers of $\mathbf{T_8}$-O_h-$\{4^6\}$.

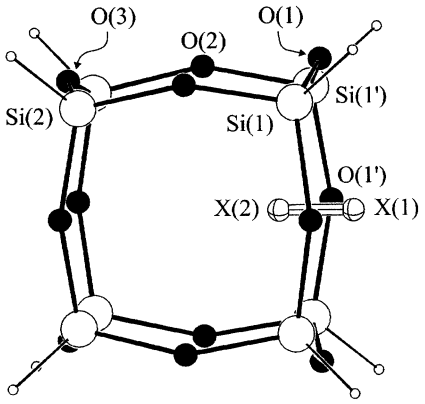

Figure 3. Transition structures for the X_2 insertion into the $\mathbf{T_8}$-POSS: N_2-C_{4v} and O_2-C_{2v}. The open circles are the silicon atoms and the filled are the oxygen atoms.

Since the main focus of this work is to assess the ability of small molecules to pass through $\mathbf{T_n}$ cages, it is interesting to consider the size of the $\mathbf{T_8}$ cage further. The Si−O distance of 1.624 Å and predicted O_h symmetry leads to a 4.442 Å distance between two diametrically opposite silicon atoms, while two opposite oxygen atoms are 3.726 Å apart. For comparison, the HF/TZV(d) interatomic distances for N_2 and O_2, are 1.068 and 1.153 Å respectively; therefore, the dimension of these molecules is small enough to fit inside a $\mathbf{T_8}$ cage. This is still the case if one considers twice the atomic radius: 1.46 and 1.50 Å for N_2 and O_2, respectively.

In addition to the octahedral structure, $\mathbf{T_8}$ has two possible isomers that show other classes of faces different from D_4. The structures of these isomers, C_{2v}-$\{3^24^25^2\}$ and D_{2h}-$\{3^46^2\}$, are shown in Figure 2.

The energies of these structures relative to the O_h structure are 12.8 and 38.8 kcal/mol for the C_{2v} and D_{2h}. isomers, respectively, due to the presence of the smaller D_3 rings.[39] So, since all of these species have a D_4 face, the $\mathbf{T_8}$-O_h system has been used as the model for the study of D_4 penetration by X_2. The larger D_5 and D_6 faces are discussed in the subsequent sections on the $\mathbf{T_{10}}$-D_{5h}, and $\mathbf{T_{12}}$-D_{6h} systems.

The transition structures for insertion of singlet N_2 and triplet O_2 are illustrated in Figure 3. While the TS for the N_2 system has C_{4v} symmetry, the O_2 structure at that symmetry is a second-order saddle point; the location of the actual O_2 TS has C_{2v} symmetry.

The presence of the N_2 molecule traversing the D_4 face of the $\mathbf{T_8}$−POSS distorts the geometry of the POSS. The N_2 bond

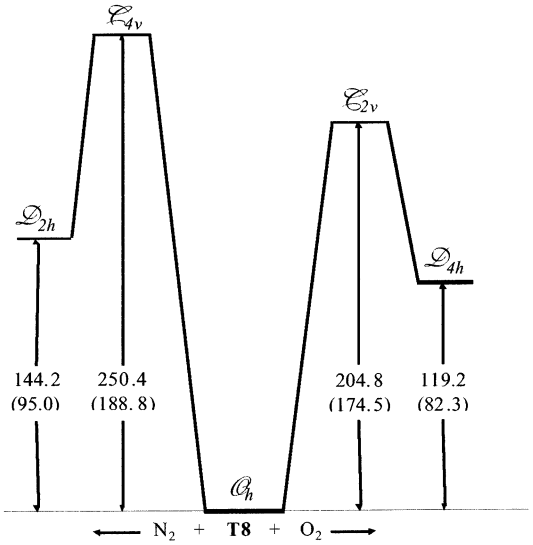

Figure 4. Interaction profile for X_2 (N_2 and O_2) insertion into $\mathbf{T_8}$. Energies are in kcal/mol. In parentheses are the MP2 single-point values.

length at the TS is the same as that in the isolated molecule (1.068 Å). However, the four Si(1)−O(1) distances (see Figure 3 for atom labeling) increase from 1.624 Å in the isolated POSS to 1.755 Å in the TS. The Si(1)−O(1)−Si(1′) angles decrease from 150.5° to 140.0° and the O(1)−Si(1′)−O(1′) angles increase from 108.4° in the POSS to 122.0° in the TS. The rest of geometrical parameters remain practically constant.

In the case of oxygen, the O_2 molecule and the POSS undergo a mutual distortion: The O−O distance elongates from 1.153 Å to 1.213 Å in the transition structure since the OO bond is weaker than NN. At the same time, the D_4 ring increases its size by stretching the Si−O(1) and Si−O(1′) bonds to 1.727 and 1.735 Å, respectively. The Si(1)−O(1)−Si(1′) decreases slightly to 144.7° and the O(1)−Si(1′)−O(1′) angles increase to 119.9° with respect to the unperturbed POSS. The reduction of the O_2::POSS TS symmetry to C_{2v} is caused by an irregular distortion of the D_4 POSS face through which the O_2 molecule penetrates. This distortion takes place through the four oxygen atoms of the D_4 ring in such a way that they separate distinctly from the center, while the four silicon atoms remain equidistant from the oxygen molecule.

Figure 4 summarizes the energy profiles for N_2 and O_2 insertion through a $\mathbf{T_8}$ D_4 face. Both barriers are very large and there is a significant correlation effect on the calculated barrier heights. At the MP2 level of theory, the barriers are 188.8 and 174.5 kcal/mol for N_2 and O_2, respectively, both very close to the Si−O bond enthalpy: 191.1 ± 3.2 kcal/mol.[40] The endothermicities of the global processes are also rather large: 95.0 and 82.3 kcal/mol for N_2 and O_2, respectively. So, it is unlikely that N_2 or O_2 will insert into $\mathbf{T_8}$ under normal conditions.

After the molecule X_2 penetrates the cage, it may adopt the three possible orientations whose structure and relative MP2 energies are illustrated in Figure 5. Each structure has been characterized as a stationary point on the PES.

The favored orientations are different for N_2 and O_2. The N_2 molecule prefers to align in a parallel arrangement relative to the opposing oxygen atoms (structure **A** in Figure 5), while O_2 is aligned perpendicular to these atoms (structure **B**) In each case, the other two arrangements are first or second-order saddle point. The clusters with the N_2 molecule aligned with two opposite silicon atoms, Figure 5, structure **C,** is the least stable. In this arrangement, the two nitrogen lone pairs point at the silicon atoms forming an apparent hypervalent coordination at

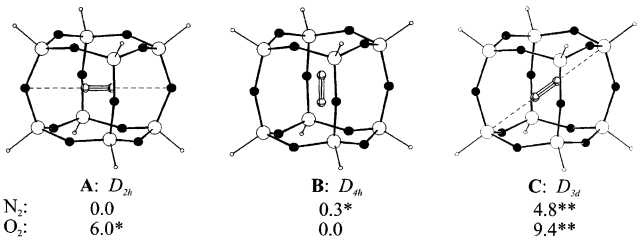

Figure 5. Structure and relative MP2 energies including ZPE correction of the three X_2::$\mathbf{T_8}$ rotamers. *: First-order saddle point. **: Second-order saddle point.

each Si. Although in the present system this interaction is forced, due to the relative dimensions of the cage plus molecule of nitrogen, such pentavalent structures are common in silicon compounds.[41]

B. $\mathbf{T_{10}}$. The POSS species of stoichiometry $(RSiO_{3/2})_{10}$, $\mathbf{T_{10}}$, is also well-known experimentally,[3,42] and theoretically.[8] The larger size of the compound compared with $\mathbf{T_8}$ might result in more isomers; however, only one, with D_{5h} symmetry and topology $\{4^55^2\}$, has been observed experimentally (see Figure 6, structure **A**).[3] To gain some insights into the experimental absence of other plausible $\mathbf{T_{10}}$ structures, two additional structural isomers have been studied (Figure 6, structures **B** and **C**). On the bases of the relative energies given in the figure, the isomers that contain D_3 faces are considerably less stable than the D_{5h} $\{4^55^2\}$ structure. This is consistent with the observation that only the latter isomer is found experimentally. In Table 2 are shown selected geometric parameters for the observed isomer, obtained from different sources. The theoretical description of this system reproduces its experimental structure reasonably well.

The $\mathbf{T_{10}}$ and $\mathbf{T_8}$ structures have similar Si−O bond lengths and angles, particularly in the atoms that construct the D_4 faces. Presumably, the energies associated with insertion into a D_4 face will be similar to those shown in Figure 4. Therefore, the insertion of N_2 and O_2 into the D_5 face is considered here.

The energy profile for the insertion of N_2 and O_2 into the $\mathbf{T_{10}}$ cage through the D_5 face is shown in Figure 8. For both molecules, the penetration occurs through a C_{5v} transition structure (Figure 7).

Since the D_5 face in $\mathbf{T_{10}}$ is larger than the D_4 face in $\mathbf{T_8}$, the insertion of a molecule X_2 is easier. This fact is reflected by the small variation of the bond length of X_2 in the transition structure. The N_2 internuclear distance changes from 1.068 Å outside the cage to 1.062 Å in the TS, and the O_2 reduces its length from 1.153 to 1.152 Å when it reaches the TS. The very small decrease in the O−O bond length here, in contrast to the large increase in this distance in the $\mathbf{T_8}$ TS, reflects the much smaller stress put on the O_2 molecule as it passes through a D_5 face. Similarly, the barriers and endothermicities for N_2 and O_2 insertion are much smaller than those calculated for the $\mathbf{T_8}$ system. The MP2 insertion barriers for N_2 and O_2 are 65.8 and 52.6 kcal/mol, respectively. Although these energies are still large, they are much smaller than the Si−O bond energy. So, these insertions may be feasible at high temperatures and/or pressures. The structures of the two X_2::$\mathbf{T_{10}}$ insertion products have D_{5h} symmetry (see structure **A** in Figure 9) and the endothermicities of formation are 24.0 and 19.2 kcal/mol for N_2 and O_2 respectively.

Besides the cluster with D_{5h} symmetry, another possible conformer with C_{2v} symmetry has been identified (Figure 9, structure **B**). It could be associated either with the internal rotation of the X_2 molecule inside the cage or with the

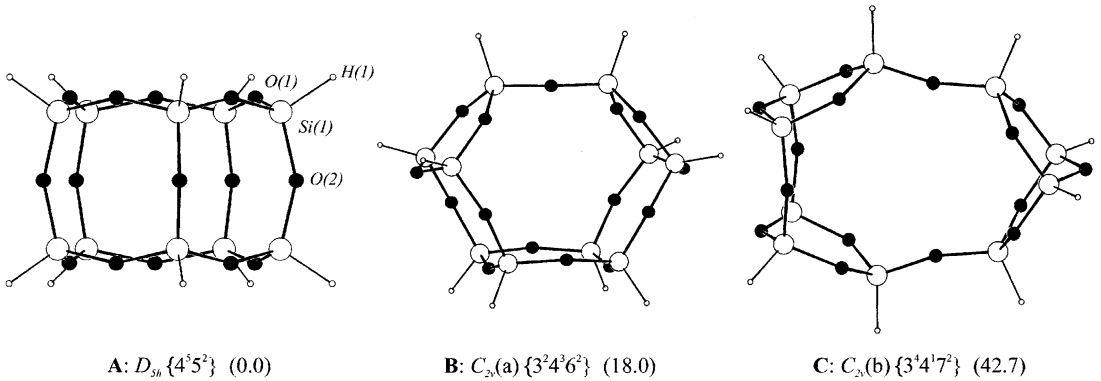

Figure 6. Three $\mathbf{T_{10}}$-POSS structural isomers. In parentheses are shown the calculated energies (kcal/mol) relative to the experimentally observed isomer.

TABLE 2: Selected Structural Parameters for T_{10}-Poss D_{5h}-{$4^5 5^2$}

	calcd[a]	exptl[b]	calcd[c]
Si−H	1.457		1.459
Si−O(1)	1.619	1.601	1.625
Si−O(2)	1.624	1.612	1.629
Si−O(1)−Si	156.3	154.7	155.3
Si−O(2)−Si	153.8	149.5	152.1
O(1)−Si-O(1′)	109.4		109.0
O(1)−Si-O(2)	108.6		109.3

[a] This work, HF/VTZ(d,p). [b] X-ray diffraction, ref 42a. [c] From ref 8b.

energetically less favorable insertion through the D_4 face. Structure **B** is less stable than structure **A** by 1.6 and 2.7 kcal/mol when X_2 is N_2 or O_2, respectively.

C. $\mathbf{T_{12}}$. As the size of the cage increases, the number of possible structures increases. Twelve T_{12} structures have been investigated (Figure 10), and the two lowest energy isomers are those with D_{2d} and D_{6h} symmetry shown in Figure 11.

As noted for the smaller $\mathbf{T_8}$ and $\mathbf{T_{10}}$ POSS, one can establish a relationship between the relative energy of two isomers and their topological structure: The more D_3 rings in the structure, the less stable it is. The exceptional instability of the D_{3h} structure (74.6 kcal/mol with respect to D_{6h}) is due to the condensation of the six D_3 faces by pairs.

At the HF level of theory, the D_{2d} structure in Figure 11 is 4.7 kcal/mol more stable than the D_{6h} structure. MP2 also favors the D_{2d} structure by ca. 1.0 kcal/mol, 1.2 kcal/mol including the ZPE correction. In the solid state, the structure of the compound determined by X-ray diffraction is D_{2d}.[43] Also, in solution, by ^{1}H NMR and ^{29}Si{^{1}H}-NMR only the species with D_{2d} symmetry has been observed, despite this apparently small difference in energy.[3,44] At the HF level of theory, Earley has estimated the difference between these isomers to 2.6 kcal/mol.[8b] The homologous isostructural titanium compound $(HTiO_{3/2})_{12}$ also has this energy order: The D_{2h} structure is 6.4 kcal/mol more stable than the D_{6h} one (3.6 kcal/mol at MP2/TZVP).[45]

Selected geometric parameters for the calculated D_{2d} and D_{6h} structures are compared with experimental data obtained from diffraction experiments in Table 3. The calculated D_{2d} geometry of {$4^4 5^4$} topology is in good agreement with experiment. The two types of silicon atoms in this species are similar; the Si−H distances are 1.459 and 1.457 Å, and the Si−O bond distances are also very close to those calculated in previous POSS. The geometric parameters that characterize the D_4 and D_5 rings in this structure are similar to those calculated for $\mathbf{T_8}$ and $\mathbf{T_{10}}$; therefore, the energetics for the insertion of X_2 through these faces should be similar to those discussed earlier.

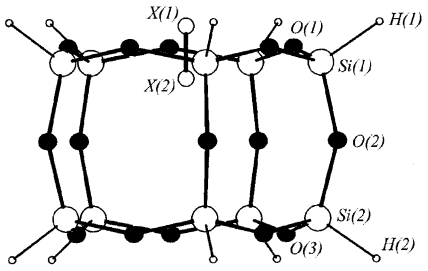

Figure 7. Calculated transition structure for the insertion of X_2 through one of the D_5 faces of D_{5h} $\mathbf{T_{10}}$.

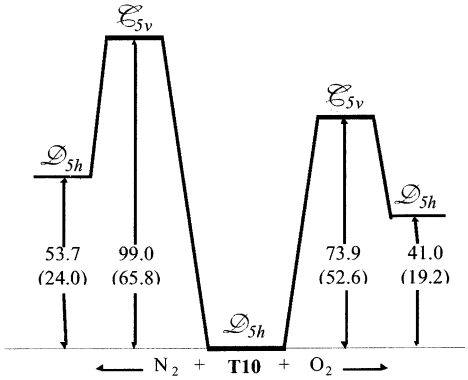

Figure 8. Energy profile for $\mathbf{T_{10}}$. Energies are in kcal/mol including ZPE correction. The MP2 values are given in parentheses.

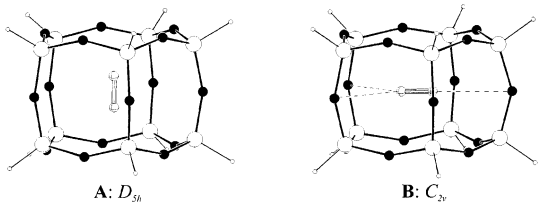

Figure 9. Orientations of X_2 inside of the POSS $\mathbf{T_{10}}$-D_{5h}.

The $\mathbf{T_{12}}$-D_{6h} structure possesses a {$4^6 6^2$} topology. Since the mechanism of X_2 insertion has already been studied for D_4 (in $\mathbf{T_8}$) and D_5 (in $\mathbf{T_{10}}$) faces, this section will focus on the same process through the D_6 ring in the $\mathbf{T_{12}}$-D_{6h}-POSS. The calculated MP2 energy profile and the symmetry of each stationary structure are presented in Figure 12.

The energy barriers are considerably lower than those calculated for $\mathbf{T_8}$ and $\mathbf{T_{10}}$. In addition, the energy differences and barrier heights for insertion into the D_6 face are now similar for N_2 and O_2. The N_2 barrier is only 4 kcal/mol larger and the insertion is slightly exothermic; the O_2 insertion is essentially thermoneutral. In both mechanisms, the transition structure has

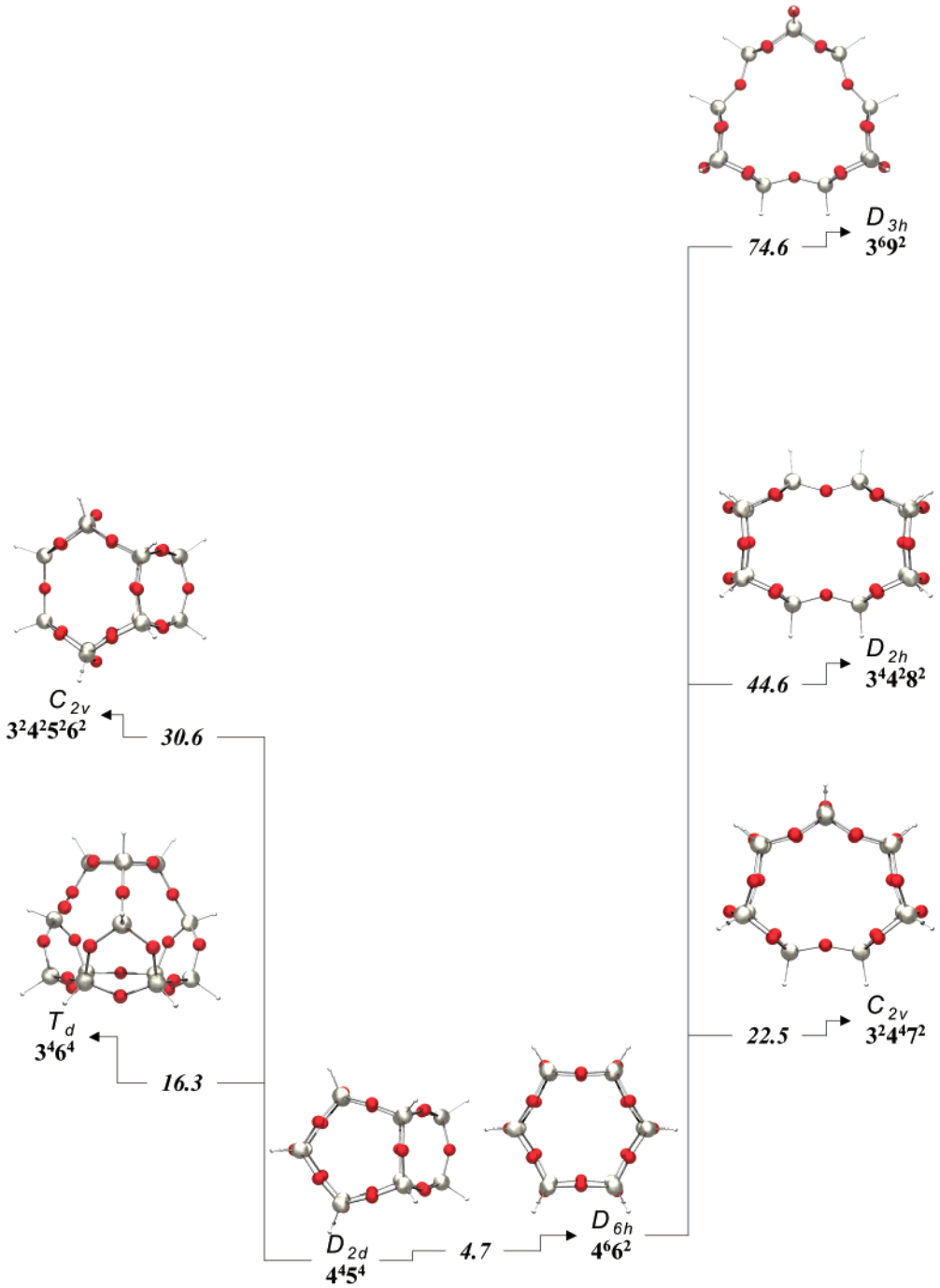

Figure 10. Structure, symmetry and topological descriptor of twelve $\mathbf{T_{12}}$ isomers. The numbers between arrows indicate the relative HF/TZV(d,p) energy in kcal/mol.

C_{6v} symmetry (Figure 13). As noted for the $\mathbf{T_{10}}$ cage, the X−X distance slightly decreases with respect to the isolated molecules: 1.068 to 1.064 Å and 1.153 to 1.151 Å for the TS of N_2 and O_2, respectively. Because of the large size of the D_6 ring, the geometrical parameters of the $\mathbf{T_{12}}$ cage do not change much due to the insertion; moreover, the structures of both N_2::$\mathbf{T_{12}}$ and O_2::$\mathbf{T_{12}}$ TS are practically identical.

Once inside the T_{12} cage, O_2 and N_2 can adopt three different orientations (Figure 14): one with D_{6h} symmetry, **C**, and two, **A** and **B**, with D_{2h} symmetry. For both N_2 and O_2, the most symmetric D_{6h} rotamer (Figure 14, structure **C**), is slightly higher in energy than the others.

When X = N, the preferred conformation has the axis of the N_2 molecule perpendicular to opposite D_4 faces of the T_{12} (Figure 14 **A**). The other D_{2h} rotamer corresponds to a transition structure. When X = O, the energetic order of the structures reverses.

Electronic and Electrostatic Implications in the Insertion Mechanism

An interesting feature of the insertion mechanism is the polarization that the inserted molecule, X2, undergoes in the TS. Table 4 summarizes the Mulliken atomic charges on the oxygen and nitrogen atoms at the transition structures. For both N_2 and O_2, the atom located inside the cage (X_{ins}) acquires a negative charge and the external atom (X_{out}) becomes positively charged. Since these charges are not equal in magnitude, there is also a net negative charge transfer to the inserting molecule.

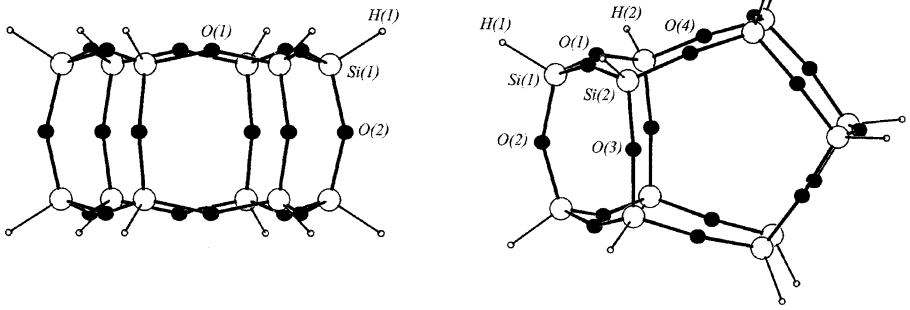

Figure 11. Structures of the two most stable $\mathbf{T_{12}}$-POSS, D_{6h}-{$4^6 6^2$}, and D_{2d}-{$4^4 5^4$}.

TABLE 3: Selected Geometrical Parameters for the Most Stable T_{12} Structures: See Figure 11 for Atom Labeling

	D_{6h}	D_{2d}	D_{2d}, exptl[b]
Si(1)−H(1)	1.459	1.458	1.460
Si(2)−H(2)		1.459	1.458
Si(1)−O(1)	1.618	1.619	1.610
Si(1)−O(2)	1.624	1.624	1.616
Si(2)−O(1)		1.620	1.603
Si(2)−O3)		1.619	1.602
Si(2)−O(4)		1.613	1.596
Si(1)−O(1)-Si(2)	108.7	157.0	152.8
Si(1)−O(2)-Si(1)[c]	154.0	152.7	151.7
Si(2)−O(3)-Si(2)		162.8	159.7
O(1)−Si(1)-O(1)	109.6	109.5	109.3
O(1)−Si(2)-O(4)		109.4	109.8

[a] Bond distances are in angstroms and angles in degrees. [b] Average X-ray values taken from ref 43c. [c] Repeated atoms indicates that they are related by symmetry.

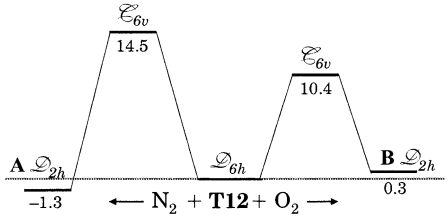

Figure 12. MP2 energy profile for the insertion of X_2 into $\mathbf{T_{12}}$-D_{6h}. See Figure 14 for the structures of species **A** and **B**.

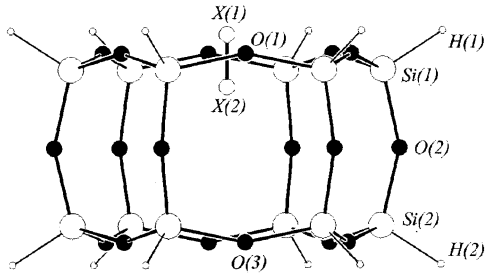

Figure 13. Calculated transition structure for the insertion of X_2 into $\mathbf{T_{12}}$-D_{6h}.

For N_2, the positive charge on N_{out} is approximately constant as the size of the cage increases, while the negative charge of the N_{ins} decreases, so that the net charge on N_2 in T_{12} is zero. However, even in this case there is a large polarization. A similar trend is observed for X = O. So, there is a net transfer of 0.1 *e* from T_8 to N_2 or O_2 at the TS, but this charge transfer decreases to approximately zero for T_{12}. On the other hand, since there is strong polarization independent of *n* in $\mathbf{T}_n$, one suspects that easily polarized molecules may insert more readily into these cages.

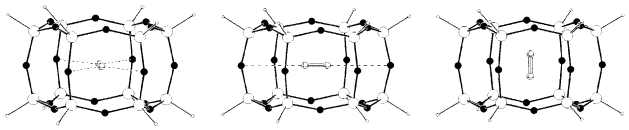

Figure 14. Structure and relative MP2 energies including ZPE correction (kcal/mol) of the three rotamers X2::$\mathbf{T_{12}}$. An asterisk indicates a structure for which the rotamer is a TS.

TABLE 4: Hartree−Fock Mulliken Charges *q* (in au) and Internuclear Distances *d* (in Å) for X_2 (N_2 and O_2) in the POSS-TS Structures

	$\mathbf{T_8}$		$\mathbf{T_{10}}$		$\mathbf{T_{12}}$	
	N_2	O_2	N_2	O_2	N_2	O_2
$d(X_2)$[a]	1.068	1.212	1.062	1.152	1.064	1.151
$q(X_{out})$	+0.136	+0.085	+0.139	+0.160	+0.142	+0.137
$q(X_{ins})$	−0.230	−0.194	−0.205	−0.188	−0.142	−0.121
$q(X_2)$	−0.094	−0.109	−0.066	−0.028	0.000	+0.016

[a] For the isolated molecules, $d(N_2)$ = 1.068 Å and $d(O_2)$ = 1.153 Å.

Conclusions

The current work assesses the possibility of inserting N_2 or O_2 into POSS cages as they pass through the faces (D_4, D_5, and D_6) of the polyhedra $\mathbf{T_8}$, $\mathbf{T_{10}}$, and $\mathbf{T_{12}}$.

The energy required to overcome the insertion barrier is close to the dissociation enthalpy of the Si−O bond when O_2 or N_2 pass through D_4 faces, but it dramatically decreases for D_5 and D_6 faces. Indeed, the insertion appears to be quite feasible through the D_6 face of $\mathbf{T_{12}}$.

Every POSS investigated shows higher permeability for O_2 than N_2 due to differences in deformability of the electron distribution of the molecular valence shell. However, this selectivity decreases as the size of the face increases: $\Delta E(D_4)$ = 14.3 kcal/mol, $\Delta E(D_5)$ = 13.2 kcal/mol, and $\Delta E(D_6)$ = 4.1 kcal/mol. Given the small difference for the D_6 of $\mathbf{T_{12}}$, it is not clear that this cage can differentiate between N_2 and O_2.

Acknowledgment. This work was supported by a grant from the Air Force Office of Scientific Research. The calculations reported here were performed on an Alpha Cluster, obtained by grants from the Department of Energy and the National Science Foundation, and on the Cray T3E at ERDC. B.T. thanks the Spanish Ministerio de Educación y Cultura for the Fellowship that has contributed to the realization of this work.

References and Notes

(1) Scott, D. W. *J. Am. Chem. Soc.* **1946**, *68*, 356.

(2) Baney, R. H.; Itoh, M.; Sakakibara, A.; Suzuki, T. *Chem. Rew.* **1995**, *95*, 1409.

(3) Agaskar, P. A.; Klemperer, W. G. *Inorg. Chim. Acta* **1995**, *229*, 355.

(4) (a) Bakhtiar, R. *Rapid Commun. Mass Spectrom.* **1999**, *13*, 87. (b) Bakhtiar, R.; Feher, F. J. *Rapid Commun. Mass Spectrom.* **1999**, *13*, 687

(5) (a) Marcolli, C.; Calzaferri, G. *Appl. Organomet. Chem.* **1999**, *13*, 213. (b) Unno, M.; Alias, S. B.; Arai, M.; Takada, K.; Tanaka, R.; Matsumoto, H. *Appl. Organomet. Chem.* **1999**, *13*, 303. (c) Krijnen, S.; Harmsen, R. J.; Abbenhuis, H. C. L.; Van Hooff, J. H. C.; Van Santen, R. A. *Chem. Commun.* **1999**, 501.

(6) Krüger, R.-P.; Much, H.; Schulz, G.; Rikowski, E. *Monatsh. Chem.* **1999**, *130*, 163.

(7) (a) Kudo, T.; Gordon, M. S. *J. Phys. Chem. A* **2000**, *104*, 4058. (b) Kudo, T.; Gordon, M. S. *J. Am. Chem. Soc.* **1998**, *120*, 11432. (c) Cypryk, M.; Apeloig, Y. *Organometallics* **2002**, *21*, 2165.

(8) (a) Jug, K.; Wichmann, D. *J. Comput. Chem.* **2000**, *21*, 1549. (b) Earley, C. W. *J. Phys. Chem.* **1994**, *98*, 8693. (c) de Man, A. J. M.; Sauer, J. *J. Phys. Chem.* **1996**, *100*, 5025 (d) Hill, J.-R.; Sauer, J. *J. Phys. Chem.* **1994**, *98*, 1238.

(9) Tossell, J. A. *J. Phys. Chem.* **1996**, *100*, 14828.

(10) Raj, R.; Riedel, R.; Soraru, G. D. *J. Am. Ceram. Soc.* **2001**, *84*, 2158.

(11) (a) Shockey, E. G.; Bolf, A. G.; Jones, P. F.; Schwab, J. J.; Chaffee, K. P.; Haddad, T. S.; Lichtenhan, J. D. *Appl. Organomet. Chem.* **1999**, *13*, 311. (b) Schwab, J. J.; Lichtenhan, J. D. *Appl. Organomet. Chem.* **1998**, *12*, 707. (c) Romo-Uribe, A.; Mather, P. T.; Haddad, T. S.; Lichtenhan, J. D. *J. Polym. Sci., Polym. Phys.* **1998**, *36*, 1867. (d) Matsuda, A.; Sasaki, T.; Hasegawa, K.; Tatsumisago, M.; Minami, T. *J. Am. Ceram. Soc.* **2001**, *84*, 775. (e) Shea, K. J.; Loy, D. A. *Chem. Mater.* **2001**, *13*, 3306. (f) Haddad, T. S.; Lichtenhan, J. D. *Macromolecules* **1996**, *29*, 7302.

(12) Raj, R.; Riedel, R.; Soraru, G. D. *J. Am. Ceram. Soc.* **2001**, *84*, 2158.

(13) Matsuda, A.; Sasaki, T.; Hasegawa, K.; Tatsumisago, M.; Minami, T. *J. Am. Ceram. Soc.* **2001**, *84*, 755.

(14) Murugavel, R.; Walawalkar, M. G.; Prabusankar, G.; Davis, P. *Organometallics* **2001**, *20*, 2639.

(15) (a) Pescarmona, P. P.; van der Waal, J. C.; Maxwell, I. E.; Maschmeyer, T. *Angew. Chem., Int. Ed.* **2001**, *40*, 740. (b) Abbenhuis, H. C. L. *Chem. Eur. J.* **2000**, *6*, 25. (c) Ducateau, R.; Cremer, U.; Harmsen, R. J.; Mohamud, S. I.; Abbenhuis, C. L.; van Saten, R. A.; Meetsma, A.; Thiele, S. K.-H.; van Tol, M. F. H.; Kranenburg, M. *Organometallics* **1999**, *18*, 5447. (d) Xiao, F.-S.; Han, Y.; Yu, Y.; Meng, X.; Yang, M.; Wu, S. *J. Am. Chem. Soc.* **2002**, *124*, 888. (e) Klunduk, M. C.; Maschmeyer, T.; Thomas, J. M.; Johnson, F. G. *Chem. Eur. J.* **1999**, *5*, 1481.

(16) (a) Zhang, C.; Babonneau, F.; Bonhomme, C.; Laine, R. M.; Soles, C. L.; Hristov, H. A.; Yee, A. F. *J. Am. Chem. Soc.* **1998**, *120*, 8380. (b) Harrison, P. G.; Kannengieser, R. *Chem. Commun.* **1996**, 415. (c) Abbenhuis, H. C. L.; van Herwijnen, H. W. G.; van Santen, R. A. *Chem. Commun.* **1996**, 1941. (d) Feher, F. J.; Tajima, T. L. *J. Am. Chem. Soc.* **1994**, *116*, 2145. (e) Feher, F. J.; Weller, K. J.; Schwab, J. J. *Organometallics* **1995**, *14*, 2009. (f) Feher, F. J.; Budzichowski, T. A. *Polyhedron* **1995**, *14*, 3239. (g) Feher, F. J.; Blanski, J. L. *J. Am. Chem. Soc.* **1992**, *114*, 5886. (h) Feher, F. J.; Newman, D. A.; Walzer, J. F. *J. Am. Chem. Soc.* **1989**, *111*, 1741. (i) Feher, F. J.; Budzichowski, T. A. *J. Organomet. Chem.* **1989**, *373*, 153.

(17) Liu, J.-C. *Appl. Organomet. Chem.* **1999**, *13*, 295.

(18) (a) Mehl, G. H.; Saez, I. M. *Appl. Organomet. Chem.* **1999**, *13*, 261. (b) Saez, I. B.; Goodby, J. W.; Richardson, R. M. *Chem. Eur. J.* **2001**, *7*, 2758. (c) Kim, K.-M.; Chujo, Y. *J. Polym. Sci., Polym. Chem.* **2001**, *39*, 4035.

(19) Cheng, W.-D.; Xiang, H.-H.; Pandey, R.; Pernisz, U. C. *J. Phys. Chem.* **2000**, *104*, 6737.

(20) Maxim, N.; Abbenhuis, H. C. L.; Stobbelaar, P. J.; Mojet, B. L.; van Santen, R. A. *Phys. Chem. Chem. Phys.* **1999**, *1*, 4473.

(21) (a) Anwander, R. *Chem. Mater.* **2001**, *13*, 4419. (b) Feher, F. J.; Blanski, R. L. *J. Chem. Soc., Chem. Commun.* **1990**, 1614.

(22) (a) Raghavachari, K.; Pasquarello, A.; Eng, J.; Hybertsen, M. S. *Appl. Phys. Lett.* **2000**, *76*, 3876. (b) Schneider, K. S.; Zhang, Z.; Banaszak Holl, M. M.; Orr, B. G.; Pernisz, U. C. *Phys. Rev. Lett.* **2000**, *85*, 602. (c) Pasquarello, A.; Hybertsen, M. S.; Car, R. *Phys. Rev., B* **1996**, *54*, R2339. (d) Banaszak Holl, M. M.; McFeely, F. R. *Phys. Rev. Lett.* **1993**, *71*, 2441.

(23) Greeley, J. N.; Lee, S.; Banaszak Holl M. M. *Appl. Organomet. Chem.* **1999**, *13*, 279.

(24) Schmid, G.; Pugin, R.; Malm, J.-O.; Bovin, J.-O. *Eur. J. Inorg. Chem.* **1998**, 813.

(25) Suzuki, F.; Nakane, K.; Yasuo, H. *J. Mem. Sci.* **1995**, *104*, 283.

(26) (a) Brinker, C. J. Sol−gel Processing of Amorphous Nanoporous Silicas: Thin Film and Bulk. In *Access in Nanoporous Materials*; Pinnavaia, T. J., Thorpe, M. F., Eds.; Plenum Press: New York, 1995; p. 123. (b) de Vos, R. M.; Verweij, H. *J. Membr. Sci.* **1998**, *143*, 37.

(27) Shanbhag, P. V.; Sirkar, K. K. *J. Appl. Polym. Sci.* **1998**, *69*, 1263.

(28) Feng, X.; Shao, P.; Huang, R. Y. M.; Jiang, G.; Xu, R.-X. *Separation and Purification Technology* **2002**, *27*, 211.

(29) Porterfield, W. W. In *Inorganic Chemistry, a Unified Approach*; Addison-Wesley Publishing Co.: Reading, MA, 1984.

(30) (a) H, O, and N: Dumming, T. H. *J. Chem. Phys.* **1971**, *55*, 716. (b) Si: McLean, A. D.; Chandler, G. S. *J. Chem. Phys.* **1980**, *72*, 5639. (c) Polarization functions have been taken from HONDO 7.0: Dupuis, M.; Watts, J. D.; Villar, H. O.; Hurst, G. J. B. *Comput. Phys. Comm.* **1989**, *52*, 415.

(31) (a) Pulay, P.; Fogarasi, G.; Pang, F.; Boggs, J. E. *J. Am. Chem. Soc.* **1979**, *101*, 2550. (b) Fogarasi, G.; Zhou, X.; Taylor, P. W.; Pulay, P. *J. Am. Chem. Soc.* **1992**, *114*, 8191. (c) Baker, J.; Kessi, A.; Delley, B. *J. Chem. Phys.* **1996**, *105*, 192.

(32) Pople, J. A.; Binkley, J. S.; Seeger, R. *Int. J. Quantum Chem.* **1976**, *S10*, 1.

(33) Fletcher, G. D.; Schmidt, M. W.; Gordon, M. S. *Adv. Chem. Phys.* **1999**, *110*, 267.

(34) Fletcher, G. D.; Schmidt, M. W.; Bode, B. M.; Gordon, M. S. *Comput. Phys. Commun.* **2000**, *128*, 190.

(35) Schmidt, M. W.; Baldridge, K. K.; Boatz, J. A.; Elbert, S. T.; Gordon, M. S.; Jensen, J. H.; Koseki, S.; Matsunaga, N.; Nguyen, K. A.; Su, S.; Windus, T. L.; Dupuis, M.; Montgomery, J. A. *J. Comput. Chem.* **1993**, *14*, 1347.

(36) Törnroos, K. W. *Acta Crystallogr.* **1994**, *B51*, 1646.

(37) Xiang, K.-H.; Pandey, R.; Pernisz, U. C.; Freeman, C. *J. Phys. Chem. B* **1998**, *102*, 8704.

(38) Auf der Heyde, T.; Bürgi, H.-B.; Bürgi, H.; Törnroos, K. W. *Chimia* **1991**, *45*, 38

(39) Jug, K.; Wichmann, D. *J. Mol. Struct. (THEOCHEM)* **1997**, *398*−*399*, 365.

(40) Kerr, J. A. in *CRC Handbook of Chemistry and Physics 1999*−*2000: A Ready-Reference Book of Chemical and Physical Data*, *CRC Handbook of Chemistry and Physics*, 81st ed.; Lide, D. R., Ed.; CRC Press: Boca Raton, FL, 2000.

(41) (a) Schmidt, M. W.; Windus, T. L.; Gordon, M. S. *J. Am. Chem. Soc.* **1995**, *117*, 7480. (b) Anglada, J. M.; Bo, C.; Bofill, J. M.; Crehuet, R.; Poblet, J. M. *Organometallics* **1999**, *18*, 5584. (c) Ignatyev, I. S.; Schaefer, H. F., III *Organometallics* **2001**, *20*, 3113. (d) Alkorta, I.; Rozas, I., Elguero, J. *J. Phys. Chem. A* **2001**, *105*, 743.

(42) (a) Heyde, T. P. E.; Bürgi, H.-B.; Bürgi, H.; Törnroos, K. W. *Chimia* **1991**, *45*, 38. (b) Auner, N.; Ziemer, B.; Herrschaft, B.; Ziche, W.; John, P.; Weis, J. *Eur. J. Inorg. Chem.* **1999**, 1087.

(43) (a) Törnroos, K. W.; Bürgi, H.-B.; Calzaferri, G.; Bürgi, H. *Acta Crystallogr.* **1995**, *B51*, 155. (b) Clegg, W.; Sheldrick, G. M.; Vater, M. *Acta Crystallogr.* **1979**, *B36*, 3162. (c) Hall, S. R.; Allen, F. H.; Brown, I. D. *Acta Crystallogr.* **1991**, *A47*, 655.

(44) (a) Agaskar, P. A.; Day, V. W.; Klemperer, W. G. *J. Am. Chem. Soc.* **1989**, *109*, 5554. (b) Feher, F. J.; Budzickhowski, T. A. *J. Organomet. Chem.* **1989**, *373*, 153.

(45) Kudo, T.; Gordon, M. S. *J. Chem. Phys. A* **2001**, *105*, 11276.